Review of Scientific Instruments

A stage-scanning two-photon microscope equipped with a temporal and a spatial pulse shaper: Enhance fluorescence signal by phase shaping

Cite as: Rev. Sci. Instrum. **89**, 123701 (2018); https://doi.org/10.1063/1.5025792
Submitted: 13 February 2018 . Accepted: 12 November 2018 . Published Online: 07 December 2018

Frederik Büchau, Alexander Patas, Yang Yang, Albrecht Lindinger, and Karsten Heyne

A stage-scanning two-photon microscope equipped with a temporal and a spatial pulse shaper: Enhance fluorescence signal by phase shaping

Frederik Büchau, Alexander Patas, Yang Yang, Albrecht Lindinger, and Karsten Heyne[a)]
Department of Physics, Free University of Berlin, Arnimallee 14, D-14159 Berlin, Germany

(Received 13 February 2018; accepted 12 November 2018; published online 7 December 2018)

Here, we present a stage-scanning two-photon microscope (2PM) equipped with a temporal pulse shaper and a spatial light modulator enabling full control over spectral and spatial phases of the exciting laser pulse. We demonstrate the capability of correcting wavefronts and temporal pulse distortions without cross-dependencies induced by optical elements at the same time enhancing the fluorescence signal. We implemented phase resolved interferometric spectral modulation for temporal pulse shaping and the iterative feedback adaptive compensation technique for spatial pulse modulation as iterative techniques. Sample distortions were simulated by cover glass plates in the optical path and by chirping the exciting laser pulses. Optimization of the spectral and spatial phases results in a signal increase of 30% and nearly complete recovery of the losses. Applying a measured spatial compensation phase within a real leaf sample shows the enhancement in contrast due to wavefront shaping with local fluorescence increase up to 75%. The setup allows full independent control over spatial and spectral phases keeping or improving the spatial resolution of our microscope and provides the optimal tool for sensitive non-linear and coherent control microscopy. https://doi.org/10.1063/1.5025792

I. INTRODUCTION

Since the presentation of two-photon microscopy by Denk *et al.*,[1] many approaches to increase the imaging quality and signal strength from within samples have been pursued.[2–5] Basically there are two possibilities, which are not mutually exclusive: increase the amount of detected photons and/or increase the amount of two-photon excited fluorescence (2PEF) photons. Our work focuses on the latter. The experimentally easiest way to increase the 2PEF is to raise the incident power, which results in an increase in the ballistic photons. At the same time, the sample is exposed to additional photons, which might result in out-of-focus 2PEF,[6] thus spreading the focal volume, or—if they do not take part in the two-photon absorption process—in an increase in photodamage.[7] More promising approaches came up with temporal pulse shaping and wavefront shaping techniques. The aim is to increase the photon flux through the focal spot and thus increase the amount of 2PEF at the focus, keeping the total amount of incident photons lower than in the ballistic compensation. To achieve this, one has to compensate for the distortions of the wavefront and of the temporal pulse shape induced by the microscope and the sample. The compensation of the setup-induced distortions can be greatly done by the manufacturer, e.g., by correction collars for wavefront and pulse compressors for temporal distortions. The sample-induced distortions are manifold and might vary strongly with the sample, as well as with the depth within the sample.[8,9]

Xu and Webb[10] stated the time-averaged fluorescence photon flux, which can be generated in a sample by a two-photon absorption process with a temporal Gaussian pulse, as

$$\langle F(t)\rangle \propto \langle P(t)\rangle^2 \cdot \mathrm{NA}^2/\tau, \tag{1}$$

where $\langle P(t)\rangle$ is the average power (not the peak power of the laser pulses), NA is the numerical aperture of the objective lens, and τ is the pulse duration of the laser pulses. Any kind of optical element or sample has, due to its dispersive index of refraction, an influence on the temporal shape of the laser pulses, even though it might only be of higher order. Thus a bandwidth-limited laser pulse will be temporally elongated and the 2PEF will be reduced; compare Eq. (1).

The effects of refractive index mismatches on the resolution and focal intensity were investigated by Egner *et al.*: using a dry objective lens, the high difference in the refractive indices of air and any kind of embedding media induces spherical aberrations to the wavefront, leading to lower intensity at the focus and a drop of resolution.[9]

Consequently, for a given microscope-objective-sample arrangement and measurements at different depths inside a sample, one needs to be able to dynamically modify the wavefront's shape and the temporal pulse shape during the measurement. By pre-compensating spatial aberrations throughout the beam path and shortening the pulse duration τ, one can effectively adapt the laser pulses to the sample characteristics [e.g., the (effective) refractive index]. Deformable mirrors as well as liquid crystal based microdisplays can easily and quickly modify the wavefront to a desired shape. The compensation of distortions of the laser pulse's temporal shape can in turn be greatly achieved by temporal pulse shapers.

Several recent publications on two-photon microscopy setups use wavefront shaping techniques to investigate the gain

a)Electronic mail: karsten.heyne@fu-berlin.de

in image quality[11] or the effect on the point-spread-function of an aberrated system.[12] Meanwhile there are even systems that are able to compensate for local wavefront distortions induced by the structure of a mouse's skull, thus being capable to image dendritic spines through an intact skull.[13] Fluorescence increase and resolution were improved by using pulse pairs, using pulse trains, and changing the laser parameters, such as the repetition rate.[5,14] However, including a temporal pulse shaper appears promising because it allows not only to compress the femtosecond laser pulses but also to introduce coherent control into multiphoton microscopy.[15] Using proper spectral phases, it is possible to selectively excite different fluorophores and thus look at multicolor stained samples without additional optics in the pathways.

The target for an optimal optical setup is to have full control over spatial and temporal properties of the light field. First successful attempts were made by Frumker *et al.*: they spread the spectral components of the pulse in the horizontal dimension, while using the vertical direction for modulation of both spectral phases and amplitudes.[16,17] However, one needs two dimensions for full spatial light field control and another dimension for frequency control.

In our setup, we combine both temporal pulse shaping and wavefront shaping, testing whether this combination can be used independently and enables us to control the wavefront, the temporal shape, and the polarization of the laser pulses. We measure the spectral and spatial phases by a Fourier transform based phase measurement technique, which is not restricted to preliminary assumptions (e.g., allowing only specific Zernike modes or orders of spectral phase for optimization or defining the position and radius of the applied phase on the wavefront shaping tool). Thus, we are able to identify the relevant temporal and spatial contributions affecting the 2PEF without restrictions.

II. METHODS

A. Setup

The completely home-built setup is based on a stage-scanning two-photon microscope (TPM) equipped with a pulse shaper (SLM-256, Cambridge Research and Instrumentation, Inc., Woburn, MA, USA), providing two independently tunable rows of 128 liquid crystal (LC) pixels arranged in series and a reflective phase only spatial light modulator (PLUTO-BB-HR, Holoeye Photonics AG, Berlin, Germany) with a resolution of 1920 × 1080 pixels. A computer-aided design (CAD) of the setup is shown in Fig. 1, which also shows the light pathways of the laser (red) and the fluorescence (green).

1. Laser system and power regulation

A Yb:KGW laser (Pharos SP, Light Conversion, Vilnius, Lithuania) is used as a light source, providing near-infrared (NIR) ultrashort laser pulses with a center wavelength of λ_c = 1028 nm at a repetition rate of f_{rep} = 100 kHz. The pulse duration is tunable between 190 fs and 10 ps by using the integrated compressor. This allows us to adjust the pulse duration, e.g., for the maximum 2PEF signal from a dye sample, which can be related to the shortest possible pulse—within the capabilities of the laser—at the sample's position [compare Eq. (1)]. It turns out to be necessary to use chirped pulses at the output of the laser to roughly compensate for group velocity dispersions induced by the optics within the pathway: particularly the objective lens with its large amount of glass affects the initial pulse duration tremendously. To control the input power, we set up a remotely controlled power regulation (PR) consisting of a λ/2-plate (WPQ05M-1053, Thorlabs GmbH, Dachau, Germany), placed in a motorized rotational stage (CONEX-AG-PR100P, Newport Co., Irvine, CA, USA), and a cube polarizer (CCM1-PBS253/M, Thorlabs GmbH, Dachau, Germany).

2. Temporal pulse shaper

After passing the PR, the light propagates through the temporal pulse shaper (TPS), set up as a symmetric 4*f* pulse shaping arrangement. The first reflective grating (10RG1200-1000-2, Newport Co., Irvine, CA, USA) disperses the spectral components along a plane parallel to the optical table. One focal length (f = 30 cm) from the grating, a cylindrical lens (LJ1212L1, Thorlabs GmbH, Dachau, Germany) focuses them to the Fourier plane, where the liquid crystal spatial light modulator (LCSLM) is placed and can be used to control the phase and polarization of the spectral components. Afterwards another pair of a cylindrical lens and a grating, each identical to

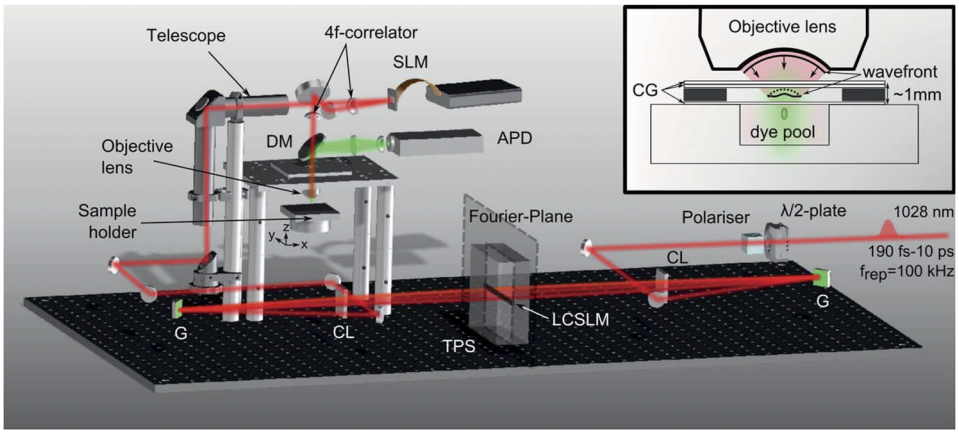

FIG. 1. CAD of the TPM equipped with a temporal and spatial pulse shaper. G: plane ruled reflection grating, CL: cylindrical lens, LCSLM: liquid crystal spatial light modulator, TPS: temporal pulse shape, SLM: spatial light modulator, DM: dichroic mirror, APD: avalanche photodiode. The laser and fluorescence light pathways are indicated in red and green, respectively. The inset shows the sample arrangement with distortions—two glued cover glasses of 170 μm thickness—placed in the pathway. For detailed descriptions of the setup, see the text.

the first, recombines the spectral components to a shaped ultrashort laser pulse. A detailed description of the pulse shaper arrangement and alignment can be found in the review article on pulse shaping of Weiner.[18]

3. Microscope with spatial pulse shaper

The shaped pulses are coupled into the microscope, where the beam diameter is expanded by using a 3:1-telescope to match the back aperture of the objective lens (LUCPLFLN 40×, NA = 0.6, Olympus K.K.,Tokio, Japan). Between the telescope and the objective, the spatial light modulator (SLM) is placed 30 cm before the entrance pupil of the objective lens. A 4*f*-correlator—built of two lenses with f = 75 mm (LA1608-B, Thorlabs GmbH, Dachau, Germany)—images the SLM surface right in front of the back aperture of the objective lens, which focuses the light into the sample. This prevents the optimization algorithm to increase the average power transmitting the objective lens at the cost of beam diameter.

4. Fluorescence collection and detector

A custom-designed 2″ dichroic mirror (Melles Griot GmbH, Bensheim, Germany), transmissive for the NIR excitation light (T > 90%) and highly reflective between 500 nm and 850 nm (R > 99%), is placed at 45° to the incoming light just before the objective lens, separating the sample's epifluorescence collected by using the objective lens from the NIR laser light and guiding it to the detector. The fluorescence is collected by a two-lens-system (LA1102-B and LA1805-B, Thorlabs GmbH, Dachau, Germany), matching the expected 10° opening angle of the fluorescence photons emerging from the exit pupil of the objective lens[19] and the detector's active area. The detector is a custom-built avalanche photodiode (APD) module (Femto Messtechnik GmbH, Berlin, Germany), equipped with a 3 mm diameter APD (S5344, Hamamatsu K. K., Hamamatsu, Japan) and switchable gain (0.05 V/nW and 0.5 V/nW). In front of the APD, a 1″ filter can be placed, which is necessary to reduce the amount of laser and stray light reaching the detector, and a short pass filter (FESH1000, Thorlabs GmbH, Dachau, Germany) is used as standard. Additionally the filter holder seals the detector from further stray light. The pulse-like fluorescence signal provided by the APD module is passed to a lock-in amplifier (LIA-MV-200-H, Femto Messtechnik GmbH, Berlin, Germany), which allows us to average the fluorescence signal over several integration times (ranging from 300 μs up to 1 s) and with different sensitivities (between 3 μV and 1 V of input voltage generating a full scale signal of 10 V at the output of the lock-in amplifier). The averaging is used for continuous measurements in scanning mode. Finally we use an analog-to-digital-converter (NI PCI-6071E, National Instruments Germany GmbH, Munich, Germany) driven by a home-built software to acquire and store the data.

5. Sample scanning stage

In contrast to many other two-photon microscopes—which use a pair of galvanometer scanners to scan the focal spot through the sample—our system is using stage-scanning. Moving the sample through the focal spot allows large area scans, not being restricted to the geometry of the objective lens. For this purpose, we use a custom-built xy-stage, based on two perpendicularly aligned ball screws (BS22-1.5 and BS22-2.0, Dr. Fritz Faulhaber GmbH & Co. KG, Schönaich, Germany), each connected to planetary gearheads (20/1 14:1, Dr. Fritz Faulhaber GmbH & Co. KG, Schönaich, Germany) and a brushless DC-servomotor (2036U024B, Dr. Fritz Faulhaber GmbH & Co. KG, Schönaich, Germany). This arrangement yields a theoretical single step resolution in the x- and y-directions of 48 nm and 36 nm, respectively. The motion of the servomotors is operated by using motion controllers (MCBL 3006 S, Dr. Fritz Faulhaber GmbH & Co. KG, Schönaich, Germany). For the axial positioning of the sample, we use a motorized lab jack (L490MZ/M, Thorlabs GmbH, Dachau, Germany), providing a theoretical resolution of <20 nm, while the supplier's software allows a minimum step size of 0.1 μm.

B. Phase measurement technique

A key role in the use of adaptive optics is the determination of the appropriate phase values. There are various publications on feedback-based methods, dealing with the increase in the intensity at the focal volume by wavefront shaping.[20–22] The review article by Vellekoop[23] summarizes the different approaches for wavefront shaping. Weiner reviewed different techniques for the TPS.[18]

Our system makes use of a feedback-based iterative method suitable for both temporal pulse shaping and wavefront shaping. It is based on the measurement of the phase of the different contributing elements—the spectral components for temporal pulse shaping and the wavefront segments for wavefront shaping—to an intensity-dependent signal. The technique was first published by Cui[21] for wavefront shaping and later adapted for temporal pulse shaping by Wu *et al.*,[24] naming it "phase resolved interferometric spectral modulation" (PRISM). Tang *et al.* used the wavefront shaping method in a two-photon-microscope, calling it "iterative feedback adaptive compensation technique" (IMPACT).[25]

The phase measurement runs as follows: we divide all available elements into a few groups and then simultaneously modulate the phases of the elements of one group, keeping the other groups at a fixed phase. These form a stationary reference field. For the modulation, unique phase ramps are randomly assigned to the elements of the modulated group. Each unique phase ramp causes the intensity-dependent signal to oscillate with a specific frequency due to the interference with the stationary reference field. The phase ramps and the total number of measured samples are selected such that the Fourier transform (FT) of the signal sequence yields amplitudes and phases at corresponding frequencies. For example, using a total number of 120 elements, divided into three groups of 40 elements, one might use the phase ramps

$$\Phi_{ramp} = \{\frac{\pi}{40+1}, 2 \cdot \frac{\pi}{40+1}, \ldots, 40 \cdot \frac{\pi}{40+1}\}, \qquad (2)$$

i.e., the phase of the ith element is increased as $\Phi_i(k) = \Phi_{ramp}(i) \cdot k$, where k is the measurement step. If we choose, for the given

example, a complete sequence to have a total number of measurement steps of $n = 2 \times (40 + 1)$, the FT contains all necessary information (Nyquist-Shannon theorem). We can immediately assign the frequencies of the FT with its amplitudes and phases to the phase ramps and thus to the elements they refer to—for PRISM and IMPACT, the frequency components of the signal's FT can be related to corresponding elements of the TPS or LCSLM, respectively.

For the given example, the lowest phase ramp examines—throughout the complete sequence—a total phase shift of 2π in equidistant phase steps. The interference of the electric field of the modulated element with the reference field causes the signal to oscillate with a specific frequency due to the ramped phase shift. The oscillation coincides with the lowest frequency (>0) in the FT of the complete sequence. The corresponding amplitude and phase can be related to its element in the modulation procedure. The second lowest phase ramp examines exactly two periods (total phase of 4π throughout the complete sequence), correlating its element to the amplitude and phase of the next frequency in the FT. Successively all other amplitudes, phases, and modulated elements are combined. This procedure is repeated for all groups one after another, to completely determine the phase values for all contributing elements. The complete algorithm can be examined iteratively: since the reference field is changed due to the adaption of the measured phase values of the contributing elements, the results of the phase measurements change iteratively. Alternative descriptions of the phase measurement algorithm can be found in the publications of Cui[21] and Wu *et al.*[24]

The amplitudes in the FT represent the relative contribution of the corresponding elements to the overall signal: in the case of PRISM, we get a scaled spectrum of our incoming light, and for IMPACT, we find the scaled transverse beam profile of the laser. More relevant for our purpose are the phases calculated by the FT: they correspond to the relative phase of the elements with respect to the reference field; i.e., applying the negative phase values to the corresponding elements, the electric fields of the elements constructively interfere with the reference field at the focus and thus we get a higher intensity compared to the non-corrected case. Ideally, we achieve constructive interference of the electric fields of all spectral components and all spatial wavefront segments at the focus within the sample.

C. Experiments

In our experiments, we investigated the potential of our two-photon microscope to increase the 2PEF from a dye pool sample using temporally and spatially shaped laser pulses. We measured the compensating phase values for the spectral components and the wavefront of the laser pulses by means of the iterative feedback algorithm outlined above.

We measured the increase in the 2PEF signal gained by phase pre-compensation on a proper dye sample: the fluorophore Nile red dissolved in ethanol. The single-photon absorption spectrum of Nile red with its maximum around λ_{max} = 520 nm seems promising to promote two-photon absorption for the given wavelength of our system. The sample used for the optimizations was prepared as a dye pool (compare the inset in Fig. 1).

The sample was placed on the sample stage right below the objective lens and raised by the lab jack to the height of a maximum signal. At this position, we expect the focal volume to be completely inside the sample and that there is least signal loss due to scattering of the fluorescence photons emerging from the sample. We further adjusted the beam path and the laser-integrated compressor to verify the maximum achievable 2PEF signal of the basic system. After finishing the adjustment, we measured the 2PEF signal in dependence of the incoming pulse energy, which we controlled by the PR. The 2PEF signal is measured as the mean of 200 measurements at a lock-in averaging time of 1 ms (see Fig. 2). This setup without the inserted cover glasses is named the undistorted case.

Afterwards we investigated the effect of the SLM and the TPS: we distorted the wavefront of the incoming light by inserting two 170 μm cover glasses (YX02.1, Carl Roth GmbH & Co. KG, Karlsruhe, Germany), glued with a glass glue, in between the sample and the objective lens, approximately 1 mm above the sample. The sample is then raised right to the same height as in the undistorted case: we call the corresponding setup the distorted case. Due to the finite amount of glass in between the objective lens and the focal plane, the effective focal distance is higher than in the undistorted case, resulting in an axial shift of the focal position (approximately 0.13 mm; compare Fig. 4). This means that for the phase correction measurements, as we performed them, the focus is not at the sample's surface but at a certain depth inside the dye pool. Thus, we leave the phase measurement algorithms space to draw the focal spot to the surface, if applicable.

At first, we optimized the temporal shape of the laser pulses with PRISM: we measured the spectral phase values for several iterations, using 120 pixels of the LCs divided into groups of 40 pixels. Without applying the spectral phase correction, we measured with IMPACT the phase values for the wavefront. Given a radial symmetry of the experiment, we reduced the modulation area for IMPACT on the SLM to a circle which we divided into squares; thus, we saved time

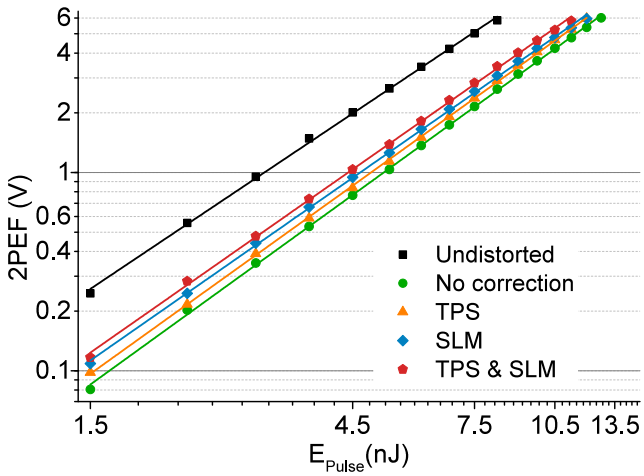

FIG. 2. 2PEF signal as a function of the incoming pulse energy (log-log-plot): the application of wavefront and spectral phase shaping each yields an increase of 2PEF and can be combined to achieve a nearly complete recovery of the 2PEF under distorted conditions.

by reducing the total number of elements in use. After five iterations, the signal increase converged to an approximately constant level. With the different possible combinations of the phase results applied to the laser pulses (spatial phase only, spectral phase only, spatial and spectral phase together), we measured the 2PEF signal in dependence of the incoming pulse energy (see Fig. 2).

The manipulation of the wavefront leads to a pre-compensation of the aberrations induced by the sample or any distortive element in the pathway; these distortions might be diversified and depend strongly upon the sample's arrangement and the sample itself. The homogeneous refractive index changes within the pathway, e.g., at the interface immersion medium/cover glass or cover glass/sample, result mainly in spherical aberration,[26–28] and non-uniformities in the refractive index of the sample may also lead to other aberrations.[29] As in two-photon microscopy, the 2PEF signal decays with the depth within the sample due to less ballistic fluorescence photons emerging from the sample's surface,[30] and the signal increase from the wavefront correction might also come from drawing the focal volume to the surface of the sample. To exclude this effect, we measured for the distorted case the z-profiles of the 2PEF signal entering the dye pool sample (z-response), with and without the correction phase. Additionally we measured the z-response of the 2PEF for the undistorted sample arrangement to quantify the depth within the sample of the phase measurements in the distorted case.

To additionally show the functionality of the TPS, we measured the compensating spectral phase values for chirped laser pulses: we tuned the compressor from its ideal position (maximum 2PEF signal) in positive and negative directions to pulse durations which yield about 70% of the maximum 2PEF signal. For both cases, we ran PRISM until the signal increase converged to a nearly constant value. We measured the 2PEF signal in dependence of the incoming pulse energy before and after applying the measured spectral phase, as well as at the ideal compressor position.

As a characterization measurement for our two-photon microscope, we determined the system's resolution by measuring the two-photon-absorption volume using a sample of 60 nm fluorescent microspheres [FS02F PS (525, 565), Bangs Laboratories, Inc., Fishers, IN, USA]. The sample was prepared following the instructions of Cole *et al.*[31]

To illustrate the effect on the imaging performance achieved by spatial phase adaption, we imaged the 2PEF at a fixed depth inside a leaf with and without a measured spatial phase correction; the leaf was mounted in between a cover glass and a microscope slide. For these measurements, we used a previous variant of the TPM setup without the $4f$-correlator.

III. RESULTS

The presented two-photon microscope with temporal and spatial pulse control starts off with the table-top laser system equipped with a pulse stretcher/compressor module, thus being capable of providing transform-limited or temporally chirped femtosecond laser pulses. After passing a combination of a rotatable $\lambda/2$-plate and a fixed polarizer—used to control the pulse's energy—the temporal shape of the light pulses is changed by using a TPS. The temporally shaped pulses are then spatially shaped by using the reflective SLM, before the light is focused into the sample by using the objective lens. The epifluorescence emitted by the sample is separated from the laser light by using a dichroic mirror, filtered by using a dielectric filter and detected by using an APD module.

The measured data for the 2PEF signal as a function of the pulse energy are shown in Fig. 2 as a log-log-plot: a slope of 2 indicates a two-photon absorption process. For the undistorted case, black squares in Fig. 2, the slope is (1.85 ± 0.02); the deviations from the ideal slope arise from saturation at high pulse energies. For all other experiments, two glued cover glasses were inserted (as shown in the inset in Fig. 1) to add distortions to the incoming wavefront (distorted case). The 2PEF signal drops to approximately 42% of the initial undistorted signal (green dots in Fig. 2). A slope of (2.00 ± 0.01) of the 2PEF signal as a function of pulse energy still indicates the two-photon absorption process.

A. Signal gain by phase compensation

With the wavefront distortion inserted, we ran PRISM for a couple of iterations to optimize the spectral phases. After three iterations, we got the maximum signal gain of about 10% (orange triangles in Fig. 2, TPS case). The two-photonic process is confirmed by the graph's slope (1.99 ± 0.01). The result of the spectral compensation phase is shown in Fig. 3(a). Applying the measured spectral phases on the laser pulses induces a temporal chirp, which compensates for high-order dispersive effects throughout the beam pathway to the sample.[18,32,33]

With the wavefront distortion inserted, but without the spectral phase compensation, we executed IMPACT to

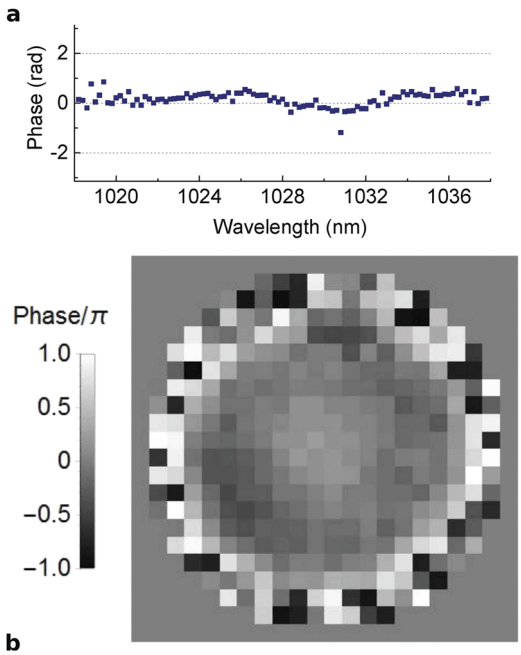

FIG. 3. Measured spectral (a) and spatial (b) phases for the distorted sample arrangement, compensating for the induced distortions of the pulse's temporal shape and wavefront, respectively.

optimize the spatial phases until the signal increase reaches its maximum at a signal gain of approximately 20% of the distorted signal. The measured spatial phase is shown in Fig. 3(b). Again the 2PEF signal (blue diamonds in Fig. 2) reveals a two-photon absorption process, indicated by the data's slope of the SLM case (1.93 ± 0.01).

Combining the spectral and spatial phase values from PRISM and IMPACT, respectively, we got a total signal gain compared to the distorted and uncorrected case of approximately 30%; the slope of the 2PEF signal for this case—TPS & SLM in Fig. 2—is (1.94 ± 0.02).

To evaluate properly the signal recovery accomplished by temporal and spatial phase shaping, we need to estimate the maximum expected 2PEF signal in the distorted case: the introduced dielectric interfaces (air-glass-air) cause intensity losses due to reflection. To estimate the intensity losses in the excitation and in the fluorescence light, we measured the intensity of the laser itself before and after inserting the glued cover glasses in the beam path, and we obtained a loss of about 10%. The signal is expected to drop to 81% due to the two-photonic dependency. Additionally we lose another 10% of the fluorescence photons due to the epifluorescence detection; thus, the expected signal with distortion reduces to 70% of the undistorted case. There is an additional signal loss due to the depth inside the sample: from Fig. 4, we can estimate this loss to be approximately 7% at a depth of 0.13 mm. Taking into account the expected losses due to the sample arrangement, we optimize the 2PEF yield close to the expected maximum.

B. Effect on axial focal position

Figure 4 shows the z-response (top) of the 2PEF recorded during the lifting of the lab jack and its derivative (bottom). At low z-position (e.g., 17.5 mm), the focus is outside the dye pool sample, and there is no 2PEF signal. Entering the sample, the 2PEF increases until the focus is completely inside the dye pool and the 2PEF signal reaches its maximum at 17.72 mm for the undistorted case. For the distorted case, the phase measurements of the sample arrangement were executed at the position of the undistorted optimal position at about 17.72 mm (relative to the lab jack's homing position). The optimal position (focus near surface and completely inside the dye pool) is found at about 17.59 mm (Fig. 4) for the distorted case, showing the expected shift of the axial focal position to a higher distance from the objective due to the introduction of a finite amount of glass ($n \approx 1.53$) in the pathway. By using the optimal position of the undistorted case as the axial position for all measurements, the phase corrections were determined approximately 0.13 mm inside the sample of the distorted sample arrangement. As can be seen from the focal position with full correction applied, the focus is not notably shifted by spatial and spectral phase optimization (Fig. 4, TPS & SLM). Moreover, the derivative of the 2PEF signal of the full correction case (green line in Fig. 4, lower panel), which can be used as an estimation of the axial resolution, shows a slight improvement of about 30% toward a higher axial resolution compared to the distorted and uncorrected focus (blue line in Fig. 4, lower panel).

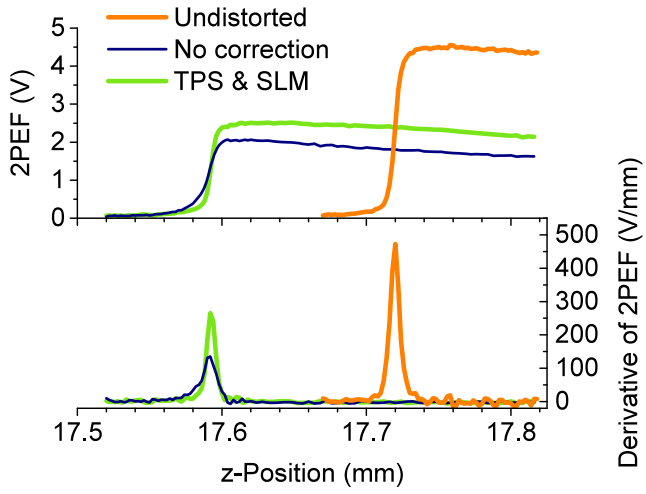

FIG. 4. The z-response of the 2PEF as a function of the lab jack's position: the orange line shows the z-response without the distortion in the beam path. Due to the cover glasses in the pathway, the focus is shifted to a lower position (higher focal distance); the blue line shows the z-response without corrections, and the green one shows the z-response with both phase corrections applied. The loss of the 2PEF signal with increasing sample depth is visible for increasing z-position.

C. Measured spectral and spatial phases

The phase corrections measured with PRISM and IMPACT after three and five iterations, respectively, are shown in Fig. 3. The spectral phase measured for the optimum position of the compressor shows a high-order correction.

To analyze the components of the spatial phase correction, we fitted the phase values to Zernike polynomials (Noll index $j \leq 24$). Since the fitting model is expected to contain too many irrelevant components, we reduced the model to the significant components by the least absolute shrinkage and selection operator (LASSO)[34] regression analysis, leaving five Zernike modes in the fitting model; the regularization parameter for the LASSO was determined by a 10-fold cross-validation. The results for the significant modes are summarized in Table I.

In Fig. 5(a), we depict the overlay of the measured spatial phase values (colored surface) and the fitted 2-dimensional model (dotted mesh) as a 3-dimensional surface plot, indicating the consistency of the fit and the measured data. To further promote the agreement, we show in Fig. 5(b) the residuals of the phases with respect to the fitted model which show only low variations and no structure across the region of interest.

Thus the most significant Zernike mode appears to be the contribution of the primary spherical. In combination with defocus, which is also present, it is expected to compensate for

TABLE I. Significant Zernike modes of the spatial phase measurement after LASSO regression analysis and their estimates from fitting the reduced model.

Noll index j	Classical name	Estimate
4	Defocus	0.48 ± 0.05
5	Oblique astigmatism	−0.72 ± 0.07
9	Vertical trefoil	0.29 ± 0.08
11	Primary spherical	1.18 ± 0.07
14	Oblique secondary astigmatism	−0.45 ± 0.09

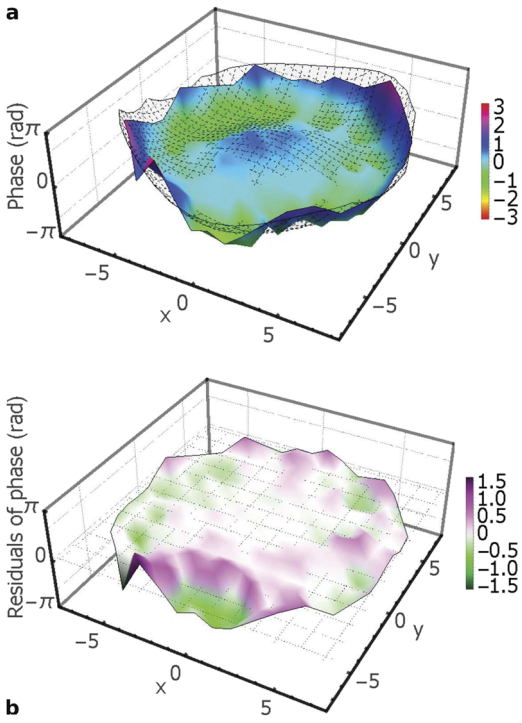

FIG. 5. The spatial phase was analyzed with LASSO regression to reduce the fit model. The mesh indicates the fit result of the reduced model, while the data are shown as a 3D profile: the fit result seems to properly coincide with the measurement (a). Also the residuals show only low variations and no structure across the region of interest; the mesh indicates the plane of zero phase residual (b).

the homogeneous refractive index mismatches throughout the laser pathway. This observation coincides with the theoretical predictions by Booth.[8] The other modes—namely, oblique astigmatism, vertical trefoil, and secondary astigmatism—are expected to arise from non-homogeneous refractive index mismatches and/or misalignments of the excitation beam pathway.

Afterwards we investigated the functionality of PRISM for a detuned compressor, i.e., for temporally chirped laser pulses. Figure 6 shows the resultant 2PEF signals linearly plot against the incoming pulse energy. For both cases, positively and negatively detuned compressors, the 2PEF signal drops due to the temporal elongation of the laser pulses at the sample (green squares and red diamonds in Fig. 6). Applying the measured phases to the TPS reveals a full recovery of the compressor- and TPS-optimized 2PEF signal for both cases (see Fig. 6, blue hexagons and orange triangles). The measured phases are summarized in Fig. 7: the offset-cleared phases show a quadratic dependence upon the wavelength, which is known as linear chirp, and can be interpreted as compression of the initially chirped laser pulses at the focal spot to a minimum pulse duration, thus yielding the highest 2PEF at the focus [compare Eq. (1)].

D. Resolution

We determined the spatial resolution of our TPM with a sample of sub-resolution fluorescent microspheres. The two-photon absorption volume was measured using a lateral step size of $\Delta x = \Delta y = 144$ nm and an interplane distance of $\Delta z = 1$ μm. The measurement is shown in Fig. 8 as stacked

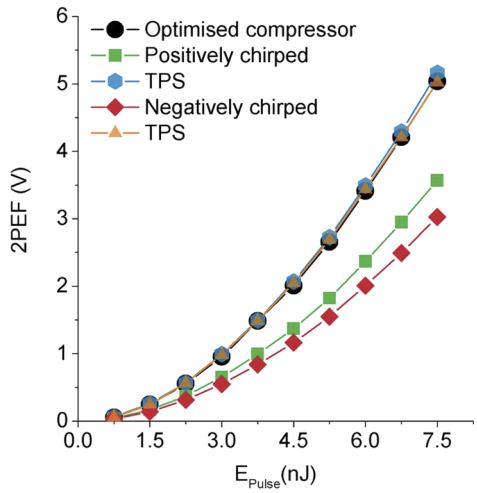

FIG. 6. 2PEF signal in dependence of the incoming pulse energy: the black circles indicate the signal for the optimized compressor position and the PRISM phase correction, shown in Fig. 3; the red diamonds and green squares show the 2PEF signals for the positively and negatively chirped pulses, while the triangles and the hexagons indicate the initially chirped but PRISM-corrected ones.

planes. The measured 4d-data $\{x, y, z, f(x, y, z)\}$ were fit to a 3-dimensional Gaussian function[35]

$$f(x,y,z) = u_0 + a_0 \times e^{-0.5\cdot(\vec{r}-\vec{r}_0)^T\cdot\boldsymbol{\Sigma}\cdot(\vec{r}-\vec{r}_0)}, \tag{3}$$

where $\vec{r}$ and $\vec{r}_0$ are the position vector and the position vector of the center of the ellipsoid, respectively, ^{T} denotes the transpose, and the symmetric matrix $\boldsymbol{\Sigma}$ represents the dimensions and orientation in space of iso-surfaces of the fitted function. Following the principal axis theorem, we get the principle axis length, by computing the inverse square root of the eigenvalues of Σ. Thus we get the resolution of our system,

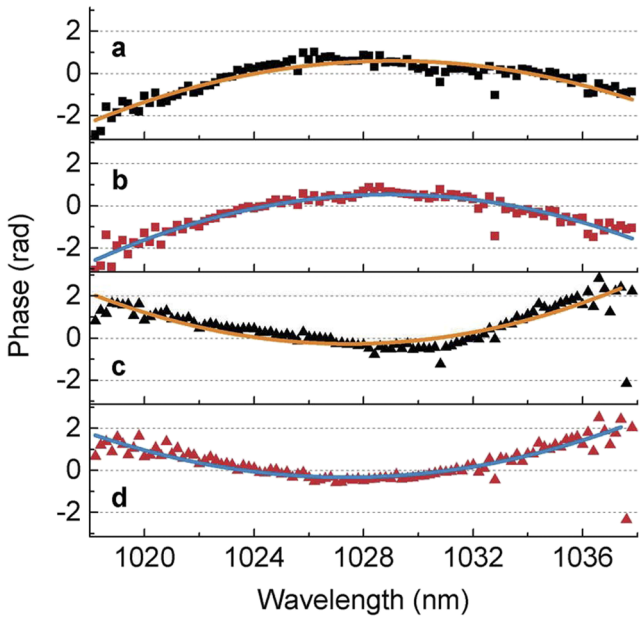

FIG. 7. The phase corrections measured with PRISM: the squares represent the positively chirped case [(a) and (b)], and the triangles represent the negatively chirped case [(c) and (d)]. In (b) and (d), the initial phase for the distorted sample arrangement, shown in Fig. 3(a), was removed, thus revealing a clear quadratic phase, i.e., a linear chirp.

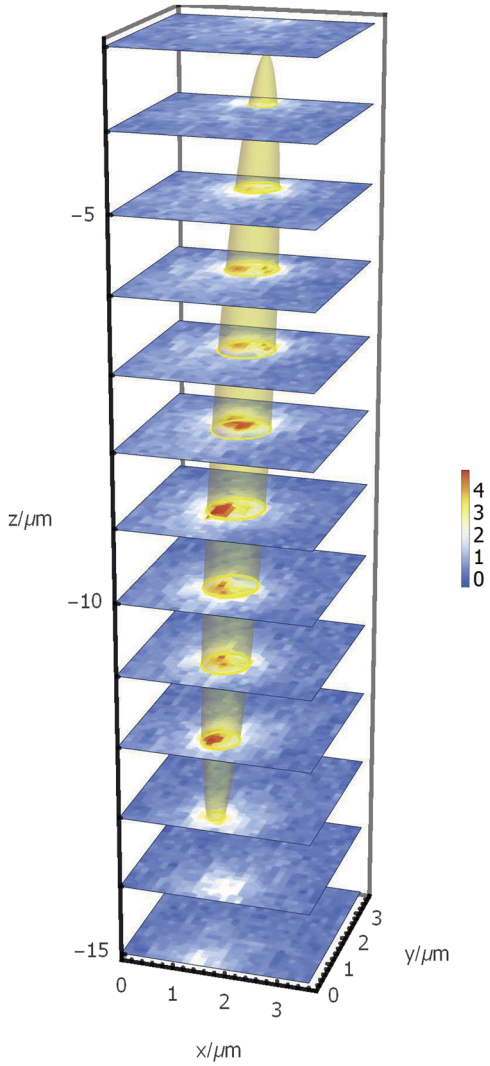

FIG. 8. The resolution imaged by a sub-resolution microsphere: the stacks were recorded at an interplane distance of $\Delta z = 1$ μm and with a lateral step size of $\Delta x = \Delta y = 144$ nm, and the yellow ellipsoid indicates the iso-surface of the FWHM of a global fit to a 3-dimensional Gaussian function, which corresponds to the resolution of the TPM.

represented by the iso-surface at the full width at half maximum (FWHM) of the given 3-dimensional Gaussian function (yellow ellipsoid shown in Fig. 8). Our measurement yields FWHM of $\Delta x = (1.0 \pm 0.2)$ μm, $\Delta y = (1.1 \pm 0.2)$ μm, and $\Delta z = (10.4 \pm 0.1)$ μm, and the transverse errors are estimated upwards from the chosen step size of the measurement, while the axial error is given by the software's precision of the lab jack's stepper motor.

E. 2PEF imaging

Finally, as an application of the 2PM with adaptive optics, we performed imaging of the 2PEF at a fixed depth within a leaf. We parked the sample at a position of the 2PEF signal and measured the spatial phase correction with IMPACT. Afterwards we measured at the same depth the 2PEF within a 122×122 μm^2 area. The measured images without and with the spatial phase compensation are shown in Figs. 9(a) and 9(b), respectively. The application of spatial

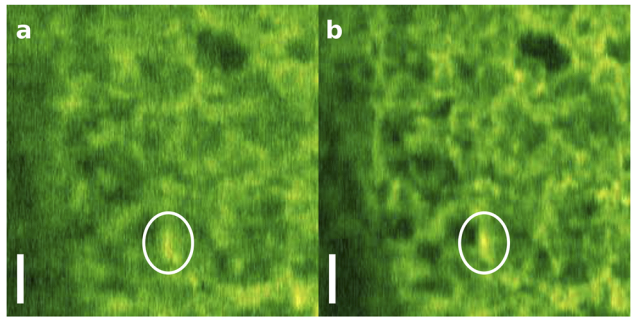

FIG. 9. Imaging of the 2PEF from a fixed depth within a leaf, taken without (a) and with (b) spatial phase compensation. The application of the measured spatial phase results in an increase in contrast; scale bar: 20 μm. The circle marks a local spot with approximately 75% signal increase.

phase compensation shows an increase in contrast with a local signal increase of up to 75%, in comparison with the non-phase-corrected 2PEF measurement.

IV. DISCUSSION AND OUTLOOK

We presented our design of a stage-scanning two-photon microscope that enables to control the spatial and temporal degrees of freedom of our femtosecond laser source. Our home-built setup is suitable for samples which do not accept immersions.

With temporal pulse shaping, we achieved a signal gain of 10% by applying spectral phases to the laser pulses by the temporal pulse shaper, although we initially optimized the pulse duration of the laser to the maximum 2PEF signal by the integrated compressor. The measured spectral phases show high-order corrections, which cannot simply be accomplished by using a standard pulse compressor. Since we used a 128 pixel SLM in the temporal pulse shaper, limiting the delay of pulse portions to approximately 0.5 ps, the effect of pulse pairs on the fluorescence could not be studied; for this investigation, a SLM with much more pixels will be needed. Additionally we were able to recover 13%–25% of the two-photon exited fluorescence signal by means of wavefront shaping, after distorting the wavefront of the incoming light by inserting a finite amount of glass in between the sample and the objective lens. We achieved this by applying a compensating spatial phase to the wavefront, which we obtained with a feedback-based optimization algorithm. The compensating spatial phase is dominated by the primary spherical mode with an additional defocus compound, as can be predicted by theoretical considerations for sample arrangements with homogeneous refractive index mismatches. Additionally there were three other significant modes identified. To give a proper estimation of the absolute gain that we accomplished with the presented phase shaping technique, one has to take into account the reflection losses of the laser and the fluorescence light by the introduced distortion, as well as the reduction of detected 2PEF due to the depth inside the sample. Considering these losses, we achieved a recovery of the estimated 2PEF close to 100%.

Shaping of spatial phases enables us to increase the contrast in real samples: we demonstrated the increase in imaging

contrast in our setup in a real leaf sample by the use of IMPACT, optimizing the spatial phases of the laser pulses. We achieved local fluorescence gain up to 75% in a leaf sample and an axial resolution increase of about 30%. With the feedback algorithm, a compensating spatial phase for every sample in every depth can be obtained.

Our laser system comes with a quite narrow bandwidth of only 8 nm; nevertheless, we were able to increase the fluorescence signal from the sample, which can directly be related to a shorter pulse length and strong focusing at the sample [see Eq. (1)]. It would be interesting to see the effort that temporal pulse shaping and PRISM yield being applied to a different laser system with a broader bandwidth, e.g., the Ti:sapphire laser usually used in two-photon microscopy.

The performed experiments suggest that it might be interesting, and at some point even necessary, to take into account spatial and spectral phase optimizations in multiphoton microscopy.[5,14] Whenever a sample is very photosensitive, one should think about the use of temporal and/or spatial phase shaping to reduce the total amount of light in use. Of course, this requires a proper consideration of the sample and of the particular measurement conditions (e.g., are there refractive index mismatches within the excitation pathway?).

Another purpose of the phase measurement techniques could be the characterization and evaluation of the performance of commercially available microscopes and of the built-in optics, as well as the development of the optics and optical systems, e.g., objective lenses for laser-based microscopy.

The measurement of the two-photon absorption volume, corresponding to the 3-dimensional resolution of our TPM, demonstrates the ability of our setup to gain full control over the spectral and spatial phases of our femtosecond laser system at high 3-dimensional spatial resolution.

There are many ways to manipulate the wavefront of a light field. Typically, micro-mirror arrays (MMA) are used to manipulate the phases of the light field.[36] The principle is based on reflection not distinguishing between different polarizations of the light field. Thus, MMAs cannot be used to generate a light field with different spectral and spatial parameters. The MMA affects all frequencies in the light field in the same way. Therefore, we used a PLUTO as a spatial light modulator which provides the interesting feature of shaping only the wavefront of one polarization direction. Since temporal pulse shapers, such as SLMs, allow for changing the polarization of individual frequencies, one can select the frequencies which are affected by the spatial light modulator. By combination of polarization shaping via the temporal pulse shaper and successive spatial light modulation, one can generate a pulse with individually manipulated frequencies and polarizations.

As an outlook, one could generate a pulse with Gaussian shape at the front and a doughnut mode at the back to set up a "one-pulse" STED (Stimulated Emission Depletion) experiment.[37] Nevertheless, the delay between the front and back of the pulse is of critical importance[14,38,39] and the complexity of the experiment will strongly increase. Here, we demonstrated the successful marriage of spatial and temporal pulse shaping for microscopy and we are looking forward to design experiments for our new setup.

ACKNOWLEDGMENTS

A.L. acknowledges the Klaus Tschira Foundation (KTS) for financial support (Project 00.314.2017).

[1] W. Denk, J. Strickler, and W. Webb, Science **248**, 73 (1990).
[2] D. Sinefeld, H. P. Paudel, D. G. Ouzounov, T. G. Bifano, and C. Xu, Opt. Express **23**, 31472 (2015).
[3] L. Sherman, J. Ye, O. Albert, and T. Norris, J. Microsc. **206**, 65 (2002).
[4] R. Turcotte, Y. Liang, and N. Ji, Biomed. Opt. Express **8**, 3891 (2017).
[5] A. K. De and D. Goswami, Int. Rev. Phys. Chem. **30**, 275 (2011).
[6] P. Theer and W. T. Denk, J. Opt. Soc. Am. A Opt. Image Sci. Vis. **23**(12), 3139–3149 (2006).
[7] K. König, "Cell damage during multi-photon microscopy," in *Handbook of Biological Confocal Microscopy*, edited by B. J. Pawley (Springer, Boston, MA, USA, 2006), pp. 680–689.
[8] M. J. Booth, "Adaptive optics in microscopy," in *Optical and Digital Image Processing* (Wiley-VCH Verlag GmbH & Co. KGaA, 2011), pp. 295–322.
[9] A. Egner and S. W. Hell, "Aberrations in confocal and multi-photon fluorescence microscopy induced by refractive index mismatch," in *Handbook of Biological Confocal Microscopy*, edited by B. J. Pawley (Springer, Boston, MA, USA, 2006), pp. 404–413.
[10] C. Xu and W. W. Webb, "Multiphoton excitation of molecular fluorophores and nonlinear laser microscopy," in *Topics in Fluorescence Spectroscopy*, Volume 5: Nonlinear and Two-Photon-Induced Fluorescence, edited by J. R. Lakowicz (Springer, USA, 2002), pp. 471–540, Book Section 11.
[11] J. M. Bueno, M. Skorsetz, R. Palacios, E. J. Gualda, and P. Artal, J. Biomed. Opt. **19**, 011007 (2014).
[12] A. Tanabe, T. Hibi, S. Ipponjima, K. Matsumoto, M. Yokoyama, M. Kurihara, N. Hashimoto, and T. Nemotoa, J. Biomed. Opt. **20**, 101204 (2015).
[13] J.-H. Park, W. Sun, and M. Cui, Proc. Natl. Acad. Sci. U. S. A. **112**, 9236 (2015).
[14] D. Goswami, D. Das, and S. Nath Bandyopadhyay, Faraday Discuss. **177**, 203 (2015).
[15] Y. Silberberg, Annu. Rev. Phys. Chem. **60**, 277 (2009).
[16] J. Vaughan, T. Hornung, T. Feurer, and K. Nelson, Opt. Lett. **30**, 323 (2005).
[17] E. Frumker and Y. Silberberg, J. Opt. Soc. Am. B **24**, 2940 (2007).
[18] A. M. Weiner, Rev. Sci. Instrum. **71**, 1929 (2000).
[19] J. P. Zinter and M. J. Levene, Opt. Express **19**, 15348 (2011).
[20] I. M. Vellekoop and A. P. Mosk, Opt. Lett. **32**, 2309 (2007).
[21] M. Cui, Opt. Lett. **36**, 870 (2011).
[22] D. B. Conkey, A. N. Brown, A. M. Caravaca-Aguirre, and R. Piestun, Opt. Express **20**, 4840 (2012).
[23] I. M. Vellekoop, Opt. Express **23**, 12189 (2015).
[24] T.-w. Wu, J. Tang, B. Hajj, and M. Cui, Opt. Express **19**, 12961 (2011).
[25] J. Tang, R. N. Germain, and M. Cui, Proc. Natl. Acad. Sci. U. S. A. **109**, 8434 (2012).
[26] S. F. Gibson and F. Lanni, J. Opt. Soc. Am. A **9**, 154 (1992).
[27] M. Booth, M. Neil, and T. Wilson, J. Microsc. **192**, 90 (1998).
[28] M. J. Booth and T. Wilson, J. Biomed. Opt. **6**, 266 (2001).
[29] M. Schwertner, M. Booth, and T. Wilson, Opt. Express **12**, 6540 (2004).
[30] F. Helmchen and W. Denk, Nat. Methods **2**, 932 (2005).
[31] R. W. Cole, T. Jinadasa, and C. M. Brown, Nat. Protoc. **6**, 1929 (2011).
[32] T. Brixner, M. Strehle, and G. Gerber, Appl. Phys. B **68**, 281 (1999).
[33] A. Monmayrant, S. Weber, and B. Chatel, J. Phys. B: At., Mol. Opt. Phys. **43**, 103001 (2010).
[34] R. Tibshirani, J. R. Stat. Soc.: Ser. B (Stat. Methodol.) **58**, 267 (1996).
[35] S. Stallinga and B. Rieger, Opt. Express **18**, 24461 (2010).
[36] Y. Song, R. M. Panas, and J. B. Hopkins, Precis. Eng. **51**, 729 (2018).
[37] A. Lindinger and K. Heyne, "Laser pulse shaping method," U.S. Patent No. 20150010029A1 (2015).
[38] A. K. De, D. Roy, and D. Goswami, J. Biomed. Opt. **15**, 060502 (2010).
[39] A. K. De, D. Roy, and D. Goswami, J. Biomed. Opt. **16**, 100505 (2011).